Available online at www.sciencedirect.com
SCIENCE DIRECT
Lithos 89 (2006) 222–241
LITHOS
www.elsevier.com/locate/lithos

Ferric iron in orogenic lherzolite massifs and controls of oxygen fugacity in the upper mantle

A.B. Woodland [a,*], J. Kornprobst [b], A. Tabit [c]

[a] Institut für Mineralogie, Universität Frankfurt, Senckenberganlage 30, D-60054 Frankfurt, Germany
[b] Laboratoire "Magmas and Volcans", CNRS-Université Blaise Pascal, 5, rue Kessler, F-63038 Clermont-Ferrand, France
[c] Department of Geology, Cadi Ayyad University, Faculty of Sciences-Semlalia, BP 2390, Marrakkech, Morocco

Received 20 May 2005; accepted 23 December 2005
Available online 6 March 2006

Abstract

The bulk Fe_2O_3 contents and inter-mineral distributions of Fe^{3+} were investigated in a suite of samples from several orogenic lherzolite massifs, including Beni Bousera (Morocco), Ronda (Spain) and Lherz (France). Ferric iron contents were determined for each phase by Mössbauer spectroscopy and these results were combined with microprobe data and modal abundances to determine the bulk Fe_2O_3 contents.

The notion that Fe^{3+} is moderately incompatible during partial melting in the mantle is supported by the observed decrease in bulk Fe_2O_3 content with increasing MgO, as well as by the generally lower Fe^{3+} content of clinopyroxene in samples with low modal abundances of this phase. The partitioning of Fe^{3+} between orthopyroxene and clinopyroxene is consistent with literature data for spinel peridotite xenoliths. The partitioning of Fe^{3+} between clinopyroxene and spinel is composition dependent, changing with the Cr/Al of spinel. Thus partitioning is expected to be different in the spinel peridotite and plagioclase peridotite facies of the upper mantle.

The fO_2 of orogenic massifs varies over several log units relative to the FMQ buffer. The values recorded by spinel-based and clinopyroxene-based oxygen barometry are generally comparable, indicating redox equilibrium between these two phases even at the relatively low temperature conditions existing in parts of the lithospheric mantle.

Calculated bulk Fe_2O_3 contents range from 0.03 to 0.27 wt.%. The combination of modal abundance and major element composition means that orthopyroxene is a major contributor to the bulk Fe_2O_3 budget of peridotites, although clinopyroxene and spinel are much richer in Fe^{3+} on a per formula unit basis. Residual Cr-rich spinel is the dominant source of Fe^{3+} in plagioclase peridotites. In terms of the geochemical behaviour of Fe^{3+}, it can be concluded that orogenic peridotites exhibit essentially the same behaviour as spinel peridotite xenoliths.

In terms of the controlling factors of fO_2 in the upper mantle, our data set records a certain degree of decoupling of fO_2 from whole rock Fe_2O_3 content, even if a correlation between these two parameters is generally apparent. This decoupling is because, whereas both whole rock Fe_2O_3 content and fO_2 are influenced by partial melting and melt extraction, additional processes such as metasomatism and phase changes can effectively reset fO_2 without always causing a concomitant change in bulk Fe_2O_3 content. Modelling the oxidation of spinel reveals that the fO_2 can be readily reset under initially reducing conditions, but the incorporation of progressively more and more Fe^{3+} in spinel is required to further raise fO_2. A quasi-limit of $\Delta \log fO_2 = FMQ + 1$ is expected.

* Corresponding author.
E-mail address: woodland@em.uni-frankfurt.de (A.B. Woodland).

doi:10.1016/j.lithos.2005.12.014

These results are consistent with the general redox behaviour observed for spinel peridotites. Our data imply that Fe^{3+}–Fe^{2+} equilibria have an important, if not dominant influence on fO_2 in the spinel peridotite facies of the upper mantle.

Keywords: Oxygen fugacity; Orogenic lherzolite massif; Mantle redox state; Mössbauer spectroscopy; Fe^{3+} in spinel; Fe^{3+} in clinopyroxene

1. Introduction

Although Fe is a major element in most mantle minerals, it is their Fe^{3+} content that determines whether Fe^{3+}/Fe^{2+} equilibria can be effective redox buffers under mantle conditions. The distribution of Fe^{3+} between phases plays a further decisive role in so much as the Fe^{3+}-concentrations and, therefore, the activities of Fe^{3+}-bearing components of the minerals are controlled in this manner. In this way, the equilibrium oxygen fugacity (fO_2) of the mantle assemblage is determined. In spite of the petrologic importance, there is a surprising lack of published data on the bulk Fe_2O_3 contents of mantle peridotites and the distribution of Fe^{3+} between coexisting phases. As a result, the geochemical behaviour of ferric iron in mantle assemblages and the influence of geochemical processes on this distribution are still only poorly known. The only comprehensive data set available is Canil and O'Neill (1996), which includes all the samples discussed in Canil et al. (1994). Based on a suite of sub-continental mantle xenoliths, Canil et al. (1994) concluded that the budgets of Fe^{3+}, C, H and S were sub-equal and that upper mantle fO_2 was unlikely to be generally controlled by any single buffer system. Data on some additional spinel peridotite xenoliths from British Columbia can also be gleaned from Canil et al. (1990) and Luth and Canil (1993). Dyar et al. (1989), McGuire et al. (1991) and Dyar et al. (1992) provide data on the inter-mineral distribution of Fe^{3+} in a total of seven spinel peridotite xenoliths mostly from the western United States, several of which were metasomatically overprinted.

In terms of the distribution of Fe^{3+}, the dominant phase in the upper mantle assemblage, olivine, is considered to contain negligible Fe^{3+} and, therefore, does not contribute significantly to the global Fe_2O_3 budget of mantle peridotites. This contention is based not only on experimental data (Nakamura and Schmalzried, 1983; Woodland and Angel, 2000), but also on crystal chemical arguments (O'Neill et al., 1993). Mössbauer spectra from clean olivine separates yield no measurable Fe^{3+} and support this conclusion (Canil and O'Neill, 1996; Woodland unpublished data). Thus it is the distribution of Fe^{3+} between orthopyroxene, clinopyroxene and spinel and/or garnet that is of interest for mantle peridotites and the redox state of the upper mantle.

Along with xenoliths, orogenic lherzolite massifs are important sources of information on mantle processes, particularly since their large size provides the opportunity to study spatial variations in structure and geochemistry at a scale of up to several km. Woodland et al. (1992) reported on the oxygen thermobarometry of Beni Bousera (N. Morocco), Ronda (S. Spain) and a number of massifs in the French Pyrenees. Their assessment was based on the Fe^{3+} contents of spinel. The purpose of this communication is to provide a detailed accounting of the bulk Fe_2O_3 contents and inter-mineral distribution of Fe^{3+} in samples from

Table 1
Samples studied and mineral modes

Sample	Whole rock	Mineral modes			
	MgO (wt.%)	Olivine	Opx	Cpx	Sp
Beni Bousera					
bbI-32e [a]	39.31	62.5	20	14.5	3
bbI-36	45.23	86	8.5	5	0.5
bbI-37 [a]	41.35	63	23	12	2
bbI-43	39.89	66	17.5	14.5	2
bbII-13	39.20	67	16	15	2
bbII-14 [a]	44.73	84	9.5	5	1.5
bbIV-11	46.22	87	7.5	4.5	1
bbV-08					
Ronda					
E3-126	44.59	82	13	4.5	0.5
E3-208 [b]	42.24	85	3	7	1
E3-227	44.20	78	15	6	1
E3-144	39.07	65	20	14	1
E3-148	38.60	61	22.5	15	1.5
Pyrenees					
Fontête Rouge					
Py-1	40.39	68	13	16	3
Lherz					
Py-18	40.49	59	24	13.5	2.5
Py-30	40.28	63	19	14	4
Py-34	39.74	65	17.5	14	3.5
Caussou					
Py-25	40.71	52.5	35	12	0.5

The bulk rock MgO content for each sample is provided.
[a] Modes by point counting, whole rock MgO estimated from modes and mineral MgO contents.
[b] Contains 4% plagioclase.

Table 2
Representative mineral compositions, including measured $Fe^{3+}/\sum Fe$ and computed Fe^{3+} cations per formula unit

Sample	BB-I-32	BB-I-32	BB-I-32	BB-I-32	BB-I-36	BB-I-36	BB-I-36	BB-I-36	BB-I-37	BB-I-37	BB-I-37
Phase	ol	opx	cpx	sp	ol	opx	cpx	sp	ol	opx	cpx
CaO	0.01	0.52	19.89		0.05	0.69	19.91		0.04	0.58	19.76
TiO_2	0.01	0.14	0.70	0.07		0.11	0.80	0.03		0.09	0.25
Cr_2O_3		0.39	0.67	7.96	0.04	0.53	0.62	8.51	0.10	0.83	1.68
MnO	0.04	0.12	0.11	0.09	0.13	0.09	0.68	0.14	0.12	0.19	0.03
FeO[a]	9.69	6.80	2.93	11.35	10.46	7.36	2.97	11.89	8.52	5.47	2.38
NiO	0.36	0.12	0.04	0.35	0.29	0.49	0.06	0.37	0.27	0.11	0.00
Na_2O		0.02	2.03	0.00		0.08	2.20	0.00	0.00	0.05	2.02
SiO_2	41.67	54.16	51.40	0.00	40.65	53.41	51.71	0.06	40.65	55.30	52.49
Al_2O_3		5.28	7.52	60.80	0.02	6.38	7.16	59.52	0.00	3.70	5.07
MgO	48.16	32.45	14.59	20.19	48.33	31.37	14.72	20.01	50.19	33.13	15.07
K_2O											
Total	99.94	100.00	99.88	100.81	99.97	100.51	100.83	100.53	99.89	99.45	98.75
$Fe^{3+}/\sum Fe$		0.028	0.136	0.103		0.022	0.097	0.129		0.057	0.065
Fe^{3+} cations[b]		0.0055 (19)	0.012 (1)	0.0249 (21)		0.0048 (21)	0.0086 (21)	0.0329 (10)		0.0091 (16)	0.0048 (5)

Sample	BB-I-37	BB-I-37	BB-I-43	BB-I-43	BB-I-43	BB-I-43	BB-II-13	BB-II-13	BB-II-13	BB-II-13	BB-II-14
Phase	sp a	sp b	ol	opx	cpx	sp	ol	opx	cpx	sp	ol
CaO				0.58	18.68		0.04	0.63	18.35		0.06
TiO_2	0.22	0.04		0.20	0.62	0.04	0.00	0.27	0.65	0.05	
Cr_2O_3	33.55	26.10	0.04	0.52	0.70	9.20	0.02	0.41	0.64	6.80	
MnO	0.28	0.15	0.14	0.17	0.04	0.15	0.16	0.16	0.08	0.08	0.16
FeO[a]	14.79	12.02	10.11	6.50	3.08	11.26	10.72	6.65	3.38	10.83	10.51
NiO	0.21	0.20	0.28	0.07	0.07	0.33	0.27	0.16	0.03	0.32	0.29
Na_2O			0.00	0.07	1.67	0.00	0.01	0.12	1.56	0.00	0.00
SiO_2	0.01	0.02	40.87	53.61	51.69	0.00	40.70	53.14	51.28	0.00	40.75
Al_2O_3	34.86	43.99	0.00	6.56	7.14	59.29	0.01	6.55	7.55	62.28	0.00
MgO	15.11	16.69	48.37	31.73	15.48	19.47	48.32	31.48	15.43	19.86	48.43
K_2O											
Total	99.03	99.21	99.81	100.01	99.17	99.74	100.25	99.57	98.95	100.22	100.20
$Fe^{3+}/\sum Fe$	0.11	0.11		0.052	0.177	0.117		0.017	0.085	0.073	
Fe^{3+} cations[b]	0.0397 (32)	0.0307 (25)		0.0099 (18)	0.0166 (5)	0.0285 (18)		0.0033 (20)	0.0087 (11)	0.0168 (9)	

Sample	BB-II-14	BB-II-14	BB-II-14	BB-IV-11	BB-IV-11	BB-IV-11	BB-IV-11	E3-126	E3-126	E3-126	E3-126
Phase	opx	cpx	sp	ol	opx	cpx	sp	ol	opx	cpx	sp a
CaO	0.62	19.03	0.01	0.04	0.68	20.93		0.02	0.73	21.03	
TiO_2	0.18	0.70	0.08	0.00	0.08	0.33	0.02	0.05	0.09	0.26	0.01
Cr_2O_3	0.33	0.61	7.43	0.10	0.36	0.70	21.94	0.03	0.73	1.56	20.09
MnO	0.16	0.30	0.15	0.15	0.17	0.12	0.15	0.17	0.23	0.08	0.20
FeO[a]	6.47	3.20	9.93	8.96	6.31	2.37	11.99	8.58	5.53	2.18	11.33

NiO	0.10	0.04	0.30	0.33	0.17	0.03	0.17	0.34	0.06	0.06	0.19
Na_2O	0.05	1.70	0.00		0.00	1.56		0.01	0.10	1.45	
SiO_2	53.57	51.09	0.00	40.51	54.75	52.80		41.25	55.42	52.24	0.03
Al_2O_3	5.79	7.81	61.59	0.03	4.48	6.21	48.10	0.01	4.46	5.88	50.15
MgO	31.46	15.12	19.93	48.68	32.79	14.95	18.22	49.40	32.79	14.78	18.66
K_2O											
Total	98.73	99.60	99.42	98.80	99.79	100.00	100.59	99.86	100.14	99.52	100.66
$Fe^{3+}/\sum Fe$	0.038	0.027	0.018		0.053	0.119	0.108		0.052	0.061	0.051
Fe^{3+} cations [b]	0.0072 (20)	0.0026 (5)	0.0043 (24)		0.0097 (18)	0.0085 (8)	0.0291 (14)		0.0083 (16)	0.0040 (6)	0.0129 (50)

Sample	E3-126	E3-144	E3-144	E3-144	E3-144	E3-148	E3-148	E3-148	E3-148	E3-208	E3-208
Phase	sp b	ol	opx	cpx	sp	ol	opx	cpx	sp	ol	opx
CaO		0.04	1.10	20.27		0.04	0.96	19.57		0.03	1.02
TiO_2	0.03	0.02	0.18	0.57	0.09	0.04	0.17	0.65	0.10	0.03	0.14
Cr_2O_3	20.66	0.03	0.46	0.83	8.86	0.03	0.42	0.74	7.74	0.00	0.66
MnO	0.14	0.20	0.23	0.11	0.13	0.18	0.12	0.18	0.12	0.16	0.18
FeO [a]	11.65	9.89	6.33	2.77	11.75	9.52	6.10	2.46	10.82	9.14	5.97
NiO	0.17	0.32			0.34	0.33			0.29	0.30	0.09
Na_2O			0.12	1.92			0.09	2.13	0.01	0.15	0.05
SiO_2		41.20	54.07	52.23	0.01	40.95	54.53	52.09	0.03	41.52	55.48
Al_2O_3	48.38	0.01	6.08	7.58	59.13	0.04	6.09	8.01	60.11	0.02	2.90
MgO	18.32	48.07	30.91	14.03	19.54	49.03	31.57	13.92	20.16	48.92	32.54
K_2O											
Total	99.35	99.78	99.48	100.31	99.85	100.16	100.05	99.75	99.38	100.27	99.03
$Fe^{3+}/\sum Fe$	0.086		0.083	0.192	0.177		0.061	0.126	0.115		0.089
Fe^{3+} cations [b]	0.0227 (53)		0.0153 (18)	0.0163 (8)	0.0450 (13)		0.0107 (18)	0.0101 (7)	0.0268 (11)		0.0155 (20)

Sample	E3-208	E3-208	E3-208	E3-208	E3-227	E3-227	E3-227	E3-227	Py-1	Py-1	Py-1
Phase	cpx	sp a	sp b	plag	ol	opx	cpx	sp	ol	opx	cpx
CaO	22.37		0.03	14.63	0.08	1.02	22.20	0.08	0.03	0.32	19.94
TiO_2	0.35	0.46	0.42	0.06	0.05	0.03	0.12	0.03	0.02	0.10	0.47
Cr_2O_3	1.35	33.67	33.08	0.01	0.00	0.75	0.95	19.83	0.04	0.29	0.80
MnO	0.03	0.18	0.17	0.00	0.11	0.09	0.06	0.08	0.12	0.12	0.05
FeO [a]	2.17	18.08	19.20	0.12	8.84	5.62	2.43	12.43	9.67	6.45	2.12
NiO	0.01	0.16	0.20		0.29	0.06	0.03	0.23	0.33	0.06	0.05
Na_2O	0.55			3.16	0.08	0.06	0.69	0.01		0.07	1.95
SiO_2	52.64		0.03	49.71	41.31	55.14	52.60	0.02	40.39	54.96	52.46
Al_2O_3	4.07	32.05	32.32	31.92	0.00	4.41	4.39	49.14	0.08	4.08	6.86
MgO	16.04	14.06	14.05	0.03	49.86	32.70	16.51	18.51	48.94	32.70	14.61
K_2O				0.00							
Total	99.58	98.66	99.50	99.64	100.62	99.88	99.98	100.36	99.62	99.15	99.31
$Fe^{3+}/\sum Fe$	0.174	0.174	0.210			0.038	0.171	0.169		0.045	0.234
Fe^{3+} cations [b]	0.0115 (5)	0.078 (9)	0.099 (10)			0.0062 (16)	0.0125 (10)	0.0484 (14)		0.0085 (18)	0.0150 (6)

(continued on next page)

Table 2 (*continued*)

Sample	Py-1	Py-18	Py-18	Py-18	Py-18	Py-25	Py-25	Py-25	Py-25	Py-25
Phase	sp	ol	opx	cpx	sp	ol	opx	cpx	sp	amph
CaO		0.03	0.41	19.69		0.02	0.42	20.95		11.63
TiO_2	0.04	0.03	0.12	0.67	0.02	0.03	0.11	0.51	0.03	3.74
Cr_2O_3	11.24	0.00	0.29	0.81	8.29	0.02	0.23	0.55	9.11	0.88
MnO	0.09	0.05	0.10	0.07	0.07	0.09	0.10	0.05	0.08	0.04
FeO[a]	12.70	9.46	6.13	2.16	12.54	10.04	6.95	2.60	14.85	4.71
NiO	0.40	0.33	0.04	0.04	0.46	0.27	0.08	0.03	0.48	0.11
Na_2O			0.06	2.09		0.01	0.03	1.68		3.50
SiO_2		41.16	54.90	52.37		40.75	55.29	52.38		42.71
Al_2O_3	57.42		4.23	7.57	60.00	0.03	3.55	5.73	57.28	14.31
MgO	18.63	51.31	33.72	14.53	19.49	49.05	33.12	14.59	18.26	16.13
K_2O										0.04
Total	100.52	102.37	99.99	99.99	100.87	100.31	99.88	99.07	100.09	97.80
$Fe^{3+}/\sum Fe$	0.140		0.067	0.239	0.212		0.054	0.318	0.267	
Fe^{3+} cations[b]	0.0388 (11)		0.0119 (17)	0.0162 (12)	0.057 (1)		0.0108 (21)	0.0252 (11)	0.087 (3)	

Sample	Py-30	Py-30	Py-30	Py-30	Py-30	Py-34	Py-34	Py-34	Py-34
Phase	ol	opx	cpx	sp a	sp b	ol	opx	cpx	sp
CaO	0.05	0.40	20.56	0.02	0.01	0.03	0.28	20.21	0.04
TiO_2	0.00	0.15	0.83	0.05	0.02		0.11	0.71	0.06
Cr_2O_3	0.00	0.18	0.72	7.89	10.74	0.00	0.29	0.69	7.25
MnO	0.14	0.22	0.08			0.17	0.17	0.03	
FeO[a]	10.26	6.62	2.22	11.60	11.81	9.59	6.54	2.50	11.52
NiO	0.51	0.08	0.02	0.41	0.25	0.38	0.11	0.11	0.30
Na_2O		0.05	2.05				0.01	1.96	0.02
SiO_2	40.99	55.55	51.59	0.04	0.03	40.09	54.93	51.75	0.01
Al_2O_3	0.00	3.56	7.24	59.30	57.43	0.00	3.80	6.74	59.83
MgO	49.75	33.69	14.27	19.96	19.56	49.56	33.74	14.51	20.02
K_2O									
Total	101.70	100.50	99.58	99.27	99.85	99.82	99.98	99.21	99.05
$Fe^{3+}/\sum Fe$		0.058	0.187	0.106	0.106		0.064	0.247	0.102
Fe^{3+} cations[b]		0.011 (2)	0.0125 (13)	0.0272 (26)	0.0266 (26)		0.0121 (18)	0.0188 (12)	0.0240 (9)

[a] Total Fe reported as FeO.

[b] Cations based upon a 6 oxygen and 4 oxygen formula unit in the pyroxenes and spinel, respectively.

several orogenic lherzolite massifs. One particular goal of this study was to determine whether or not clinopyroxene and spinel in orogenic peridotites coexist in redox equilibrium with each other. This is a potentially important point because of the long and complex emplacement histories of these massifs and since equilibration temperatures for orogenic massifs are generally significantly lower than those recorded by mantle-derived xenoliths (e.g. Fabriès et al., 1991). A further point is to use our data to discuss of the factors controlling the fO_2 in the spinel peridotite facies of the upper mantle.

2. Samples studied

A total of 17 samples were investigated in this study from the Beni Bousera, Ronda, Lherz, Fontête Rouge and Caussou orogenic lherzolite massifs. For general petrologic and geochemical descriptions of these massifs the reader is referred to Kornprobst (1969) and Pearson et al. (1993) for Beni Bousera, Obata (1980), Frey et al. (1985), Van der Wal and Vissers (1996) and Lenoir et al. (2001) for Ronda, and Conquéré (1977, 1978), Conquéré and Fabriès (1984), Bodinier et al. (1987), Fabriès et al. (1991) for the Pyrenean massifs. Some petrologic data, including estimates of oxygen fugacity, for a sub-set of these samples were reported by Woodland et al. (1992). The samples, along with their location and modal mineralogy are listed in Table 1. The samples are essentially spinel lherzolites that exhibit variable degrees of depletion, as indicated by the range in whole rock MgO content and the Cr/(Cr+Al), or $Cr^{\#}$ of the spinels (Table 2). One sample with Cr-rich spinel, E3-208, is a plagioclase-bearing lherzolite collected in the lower unit of the Ronda massif, considered to be "neo-asthenosphere" by Lenoir et al. (2001). Sample Py-25, from Caussou, has been metasomatised by a mafic silicate melt, as revealed by the presence of amphibole, light REE enrichment and elevated Li contents in clinopyroxene (Fabriès et al., 1989; Seitz and Woodland, 2000). Sample Py-18 from Lherz contains minor apatite and secondary spinel, indicative of another type of metasomatic agent, possibly a carbonatitic melt (Woodland et al., 1996).

3. Analytical methods

Mineral compositions were determined with two microprobes. Most samples were analysed on a Camebax Micro microprobe at the Université de Clermont-Ferrand II, using a 15 kV accelerating voltage an sample current of ~11 nA. Other samples were analysed on a Cameca SX-50 at the Bayerisches Geoinstitut, Bayreuth, Germany, operating at 15 kV and 20 nA. A mix of natural and synthetic standards was employed that yielded reliable results for the mantle phases analysed in this study. The analyses were all performed in wavelength-dispersive mode. A ZAF or PAP matrix correction was applied to the raw data collected on the Camebax or SX-50 microprobe, respectively.

Mineral modes were mostly derived by least squares regression, fitting mineral compositions to the whole rock composition for each sample. Whole rock analyses were performed by X-ray fluorescence analysis at the Mineralogisches Institut, Universität Heidelberg. Measurements were made on glass discs prepared using standard methods by melting rock powders with Li-borate flux. Whole rock compositions of samples E-144 and E-148 were taken from Li (1991). Due to the unavailability of rock powders, the modes of three samples (bbI-32e, bbI-37, and bbII-14) were estimated by thin section point counting.

The $Fe^{3+}/\sum Fe$ measurements were performed by ^{57}Fe Mössbauer spectroscopy at the Bayerisches Geoinstitut and at the University of Frankfurt on optically pure handpicked mineral separates. The spinels were washed in dilute HCl to remove any late stage magnetite that may have formed on the spinel surfaces during serpentinisation. Sufficient material was finely ground to prepare an absorber with a thickness of ~5 mg Fe/cm^2. Depending on the amount of material available, samples were either mounted in an acrylic holder or in a hole drilled in a Pb disc. In some cases, a small amount of benzophenone or sugar was added to yield enough material to uniformly cover the sample holder and yet retain the desired thickness. Spectra were obtained at room temperature, in transmission mode on a constant acceleration Mössbauer spectrometer with a nominal 50 mCi ^{57}Co source in a 6 μm Rh matrix. The velocity scale was calibrated relative to 25-μm-thick α-Fe at room temperature using the positions certified by NIST. Mirror image spectra were collected over 512 channels with a velocity range of ±5 mm/s. The spectra were fit with the NORMOS software package (distributed by Wissenschaftliche Elektronik GmbH, Germany). Some spectra were also fit using the program PC-MOS (provided by CMTE Elektronik, Germany), which yielded essentially the same hyperfine parameters and area ratios as those derived from the NORMOS-fit when the same spectral model was employed.

For the most part, uncertainties in $Fe^{3+}/\sum Fe$ are estimated to be ±0.01–0.02 in absolute terms. As observed by Canil and O'Neill (1996), $Fe^{3+}/\sum Fe$

calculated for orthopyroxene are generally low and at $Fe^{3+}/\sum Fe < 0.05$ different fits yielded somewhat different values, suggesting a higher degree of uncertainty, even if a small Fe^{3+} component is clearly apparent in the spectra. However, since the same fitting model was used for all orthopyroxene samples, relative differences between samples should be more robust. An uncertainty of ±0.01 in $Fe^{3+}/\sum Fe$ has been assumed for all orthopyroxene spectra. Uncertainties in the hyperfine parameters are variable depending on the degree of peak overlap and relative intensity of the doublet. For the Fe^{2+} doublets, the uncertainty is generally ±0.02 mm/s. The same uncertainty is obtained for the Fe^{3+} doublets as long as a portion of the doublet is reasonably resolved, otherwise uncertainties can be larger.

4. Results and discussion

4.1. Mineral chemistry

4.1.1. Major elements

The major element compositions of olivine, orthopyroxene, clinopyroxene and spinel are typical for mantle-derived spinel peridotites (Table 2). For example, the forsterite content of olivine has a range of $X_{fo} = 0.89$–0.91 in this suite of samples. Orthopyroxene has a similar X_{Mg} ($Mg/(Mg+Fe_{total})$) as olivine. Coexisting clinopyroxenes have predictably higher X_{Mg}; 0.92–0.94 in samples from Ronda and the Pyrenean massifs and 0.90–0.93 in the Beni Bousera samples. The X_{Mg} values of the coexisting silicate minerals are strongly correlated with each other, indicating that the samples are well equilibrated in terms of their Mg and Fe distribution. Sodium contents in clinopyroxene generally lie between 1.5 and 2.2 wt.% Na_2O (Table 2). Clinopyroxenes in two samples from Ronda have distinctly low Na_2O contents; one of these samples is the plagioclase-bearing peridotite.

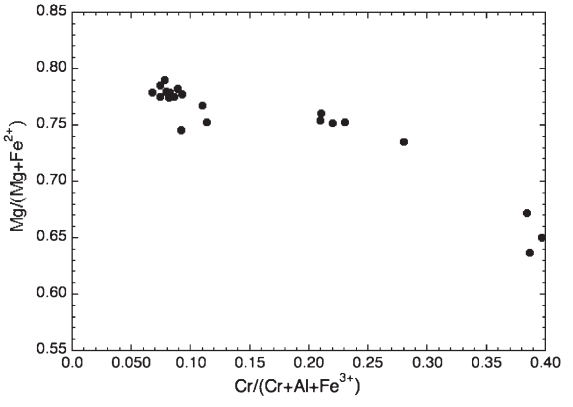

Fig. 1. Spinel composition plotted in terms of $Cr/(Cr+Al+Fe^{3+})$ vs. $Mg/(Mg+Fe^{2+})$.

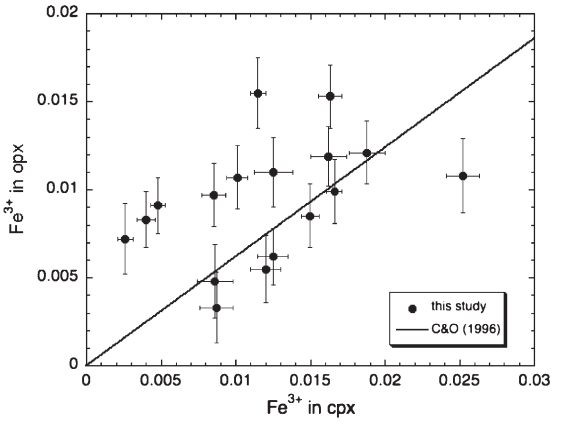

Fig. 2. Partitioning of Fe^{3+} between clinopyroxene and orthopyroxene (cations per formula unit). The line is the empirical distribution coefficient $D^{opx/cpx}_{Fe3+} = 0.62(4)$ derived by Canil and O'Neill (1996). Because of the limited resolution of the orthopyroxene spectra, an error in Fe^{3+} for this phase was calculated assuming an uncertainty ±0.01 in the measured $Fe^{3+}/\sum Fe$.

The $Cr/(Cr+Al+Fe^{3+})$ in spinel ranges from 0.07 to 0.40 with a concomitant decrease in $Mg/(Mg+Fe^{2+})$ from 0.79 to 0.63 (Fig. 1). The compositional range is attributable to variable degrees of melt extraction experienced by the individual samples, with higher Cr-contents representing higher degrees of melting (e.g. Dick and Fisher, 1984). As expected, spinels in the plagioclase-bearing sample (E3-208) are Cr-rich, owing to their residual nature during plagioclase formation. The $Cr/(Cr+Al+Fe^{3+})$ in spinel varies systematically with the X_{Mg} of the coexisting silicates and $Cr/(Cr+Al+Fe^{3+})$ in clinopyroxene, providing further evidence that these samples are well equilibrated.

4.1.2. Fe^{3+} contents in pyroxenes

The measured $Fe^{3+}/\sum Fe$ in orthopyroxene and clinopyroxene vary widely between samples in our suite (Table 2). As found in other studies of mantle peridotites, orthopyroxene has the lowest $Fe^{3+}/\sum Fe$ (Dyar et al., 1989; McGuire et al., 1991; Luth and Canil, 1993; Canil and O'Neill, 1996). Clinopyroxene exhibits a much larger range in $Fe^{3+}/\sum Fe$ from 0.02 to 0.30. Comparison of such "raw data" can be misleading, however, since the major element compositions of the phases are not considered. For example, the relatively high total iron contents in orthopyroxene mean that this phase can have a significant Fe^{3+} content, occasionally exceeding that of the coexisting clinopyroxene (see Fig. 2).

There is a tendency for clinopyroxene to have lower a Fe^{3+} content in samples that have lower modal abundances of this phase (Fig. 3A). This is consistent with the notion that Fe^{3+} is moderately incompatible during partial melting in the mantle. The fact that this tendency is not a strong correlation indicates that a variety of other factors have played a role in determining the Fe^{3+} content of clinopyroxene, including variable major element composition and equilibration temperatures between samples, metasomatic effects, as well as fO_2. For example, the sample in our suite with the highest Fe^{3+} content in clinopyroxene, Py-25, has undergone metasomatism by a mafic silicate melt (Fabriès et al., 1989; Seitz and Woodland, 2000).

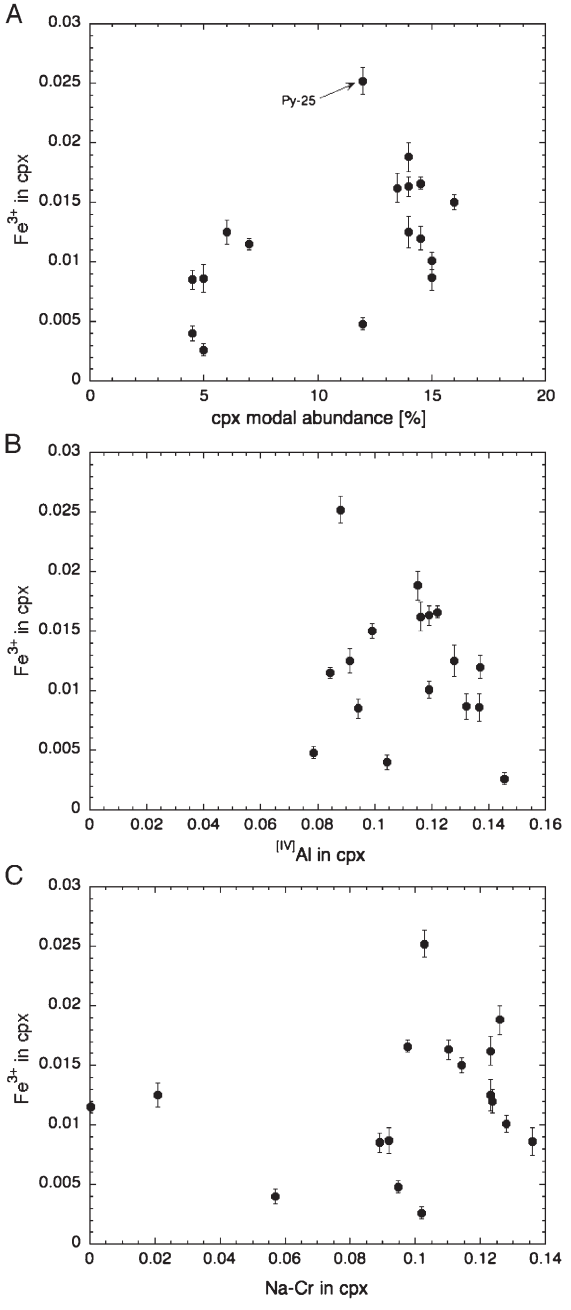

Fig. 3. Variation in Fe^{3+} concentration in clinopyroxene plotted as a function of (A) modal abundance of clinopyroxene, (B) Na–Cr and (C) tetrahedral Al contents (all as cations per formula unit). See text for discussion.

The incorporation of Fe^{3+} in both orthopyroxene and clinopyroxene can occur by a variety of charge-coupled substitution mechanisms, including the coupling of Fe^{3+} with Na on the M1 and M2 octahedral sites, respectively, as an aegerine component ($NaFe^{3+}Si_2O_6$). Another possibility could involve an essenite ($CaFe^{3+}AlSiO_6$) or similar component, where charge compensation occurs by the substitution of Al of Si on the tetrahedral sites. The absence of any correlation between Fe^{3+} and either Na or tetrahedral Al contents in clinopyroxene suggests that no single substitution mechanism is responsible (Fig. 3B, C). In Fig. 3B, the number of Na cations per formula unit plotted has been reduced by the amount of Cr in the clinopyroxene to account for the competing kosmochlor ($NaCrSi_2O_6$) component (e.g. Kornprobst et al., 1981). A further possibility is a "ferri-Tschermaks" component where Fe^{3+} simultaneously enters the M1 and tetrahedral sites (e.g. a $CaFe^{3+}_2SiO_6$ component, Huckenholz et al., 1969). This later type of substitution is certainly feasible considering that the number of tetrahedral sites available, as determined by subtracting the Si cations from two cations per formula unit, easily exceeds the amount of Fe^{3+} present. Unfortunately the resolution of the Mössbauer spectra is not sufficient to be able to distinguish between tetrahedrally and octahedrally coordinated Fe^{3+}, making unambiguous identification of a ferri-Tschermaks component problematic. Of course from a thermodynamic point of view, all potential exchange components need to be considered; these being related through a set of reciprocal reactions.

4.1.3. Fe^{3+} contents in spinel

The coexisting spinels have similar $Fe^{3+}/\sum Fe$ values to those of clinopyroxene (0.02–0.26, Table 2). The often-observed positive correlation between Fe^{3+} and Cr/(Cr+Al) in spinel (e.g. Woodland et al., 1992; Canil and O'Neill, 1996) is less clear in this suite due to a variety of competing factors operating during the complex history of these massifs. Although Fe^{3+}–Cr spinels are thermodynamically favoured over

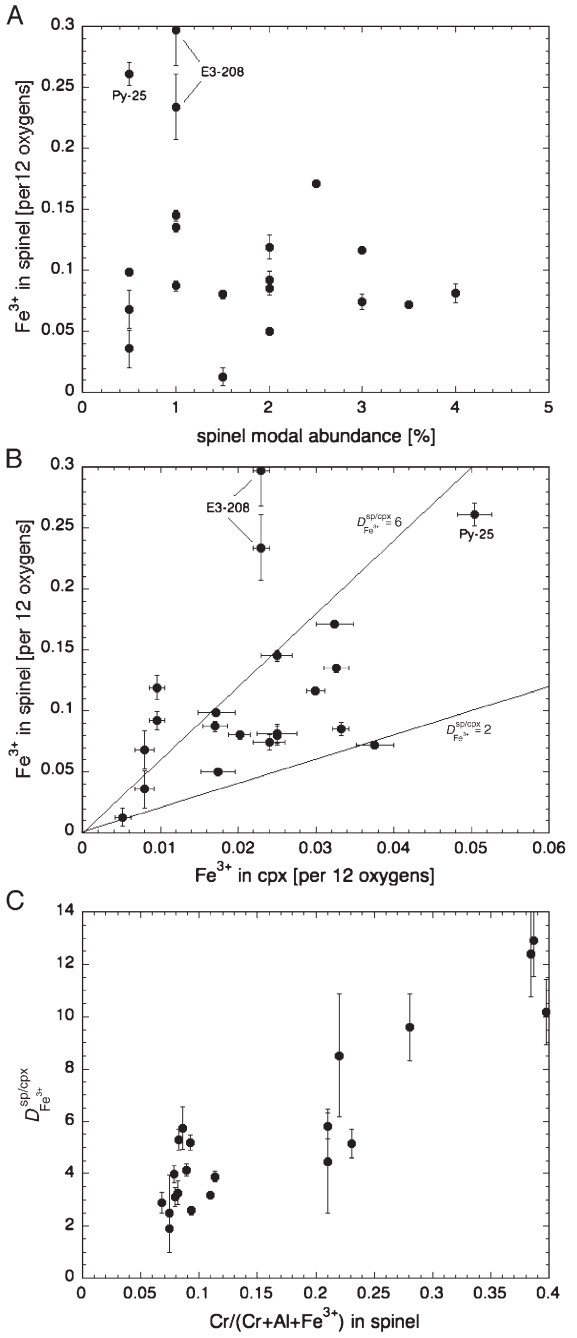

Fig. 4. (A) Fe^{3+} in spinel plotted as a function of spinel modal abundance. Fe^{3+} contents are cations per 12 oxygen formula unit. Sample E3-208 is a plagioclase-bearing peridotite and sample Py-25 has been metasomatised (see text). (B) Partitioning of Fe^{3+} between clinopyroxene and spinel. To afford a better comparison, data for both phases are plotted on the basis a 12 oxygen formula unit. The two lines depict $D^{sp/cpx}_{Fe3+}=2$ and 6, respectively. (C) Variation in the partition coefficient $D^{sp/cpx}_{Fe3+}$ as function of $Cr/(Cr+Al+Fe^{3+})$ in spinel.

Fe^{3+}–Al spinels (O'Neill and Wall, 1987), increasing Cr contents in spinel generally reflect higher degrees of depletion in mantle peridotites, which is expected to result in a progressive removal of Fe^{3+} (Bryndzia and Wood, 1990; Woodland et al., 1992). In addition, there are effects due to equilibration temperature, phase changes (i.e. spinel to plagioclase facies) and metasomatism (see below). The absence of any relationship between Fe^{3+} content and modal abundance of spinel, is a further reflection of the geochemical and petrological complexities of the lithospheric mantle (Fig. 4A).

4.2. Thermometry

Equilibration temperatures were determined using the two-pyroxene thermometer (BKN) of Brey and Köhler (1990). A pressure of 15 kb was assumed for all samples except those from Ronda, where a pressure of 9 kb was assumed (see Woodland et al., 1992). Calculations were made with all Fe assigned to Fe^{2+}. The BKN thermometer is quite insensitive to the effects whether Fe^{3+} is explicitly accounted for or not (Canil and O'Neill, 1996). However, it is important to recognise that highly oxidised samples may not be suitable for thermobarometric analysis since the mineral compositions can deviate significantly from those used in the calibration experiments. Calculated temperatures range from 833 to 1137 °C, with most samples yielding temperatures below 1000 °C (Table 3). Application of the olivine–spinel thermometer of Li et al. (1995) yields a similar range in temperatures from 840 to 1005 °C. Fairly low equilibrium temperatures are typical for massif peridotites (e.g. Fabriès et al., 1991; Woodland et al., 1992). The similarity in equilibration temperature for many samples in this suite is consistent with the roughly linear array depicted in Fig. 2, illustrating the co-variation in $Cr/(Cr+Al+Fe^{3+})$ and $Mg/(Mg+Fe^{2+})$ in spinel (e.g. Fabriès, 1979; Li et al., 1995). The samples recording high temperatures are from the Beni Bousera massif, a massif known for occasionally preserving high equilibration temperatures (Kornprobst, 1969).

4.3. Systematics of Fe^{3+} partitioning

The partitioning of Fe^{3+} between orthopyroxene and clinopyroxene is illustrated in Fig. 2. The data in this study are consistent with the empirical distribution coefficient $D^{opx/cpx}_{Fe3+}=0.62(4)$ derived by Canil and O'Neill (1996), albeit with considerable scatter. Some of the scatter is no doubt attributable to the uncertainties

Table 3
Mössbauer hyperfine parameters for spinel, clinopyroxene and orthopyroxene

	Fe^{2+}			Fe^{2+}			Fe^{2+}			Fe^{2+}			$Fe^{3+}/\sum Fe$	χ^2
	IS	QS	FWHM	IS	QS	FWHM	IS	QS	FWHM	IS	QS	FWHM		
Spinel[a]														
Beni														
bbI-32e	0.88	1.57	0.31	0.86	0.87	0.31				0.29	0.74	0.27	0.103 (9)	0.96
bbI-36	0.91	1.61	0.23	0.90	0.86	0.23				0.31	0.80	0.32	0.129 (4)	0.96
bbI-37	0.88	1.69	0.15	0.87	0.89	0.15				0.31	0.64	0.27	0.110 (9)	0.95
bbI-43	0.91	1.38	0.20	0.86	0.75	0.20				0.30	0.78	0.27	0.117 (7)	0.94
bbII-13	0.91	1.39	0.27	0.89	0.76	0.27				0.31	0.80	0.26	0.073 (4)	1.07
bbII-14	0.87	1.50	0.29	0.87	0.79	0.29				0.33	0.73	0.15	0.018 (9)	0.95
bbIV-11	0.91	1.67	0.24	0.91	0.88	0.24				0.31	0.74	0.32	0.108 (6)	0.97
Ronda														
E3-126	0.92	1.59	0.36	0.91	0.84	0.36				0.32	0.74	0.30	0.075 (3)	1.24
E3-208	0.92	1.65	0.10	0.93	0.82	0.10				0.34	0.66	0.29	0.255 (9)	1.04
E3-227	0.91	1.65	0.20	0.91	0.86	0.20				0.33	0.73	0.28	0.169 (5)	0.95
E3-144	0.91	1.67	0.23	0.90	0.91	0.23				0.31	0.78	0.30	0.177 (5)	1.08
E3-148	0.91	1.46	0.22	0.89	0.78	0.22				0.31	0.79	0.27	0.115 (5)	1.07
Pyrenees														
Py-1														
Py-18	1.12	1.79	0.26	1.07	1.02	0.26				0.38	0.96	0.38	0.212 (4)	1.11
Py-25	0.92	1.66	0.18	0.92	0.85	0.18				0.32	0.77	0.36	0.267 (9)	0.72
Py-30	0.92	1.64	0.22	0.90	0.87	0.22				0.33	0.80	0.27	0.106 (10)	1.13
Py-34	0.91	1.48	0.25	0.90	0.79	0.25				0.32	0.78	0.26	0.102 (5)	1.05
Clinopyroxene														
bbI-32e	1.14	1.95	0.40	1.17	2.30	0.42				0.27	0.80	0.67	0.136 (11)	1.53
bbI-36	1.14	2.07	0.42	1.15	2.60	0.39				0.39	0.38	0.65	0.096 (14)	1.07
bbI-37	1.15	2.09	0.41	1.15	2.72	0.22				0.23	0.35	0.24	0.065 (10)	1.14
bbI-43	1.14	2.07	0.42	1.20	2.45	0.37				0.27	0.43	0.75	0.177 (18)	1.23
bbII-13	1.14	2.01	0.41	1.18	2.37	0.45				0.25	0.35	0.67	0.085 (11)	1.16
bbII-14	1.15	2.06	0.39	1.17	2.53	0.37				0.22	0.35	0.20	0.026 (5)	1.42

(continued on next page)

Table 3 (*continued*)

	Fe^{2+}			Fe^{2+}			Fe^{2+}			Fe^{2+}			$Fe^{3+}/\sum Fe$	χ^2
	IS	QS	FWHM	IS	QS	FWHM	IS	QS	FWHM	IS	QS	FWHM		
bbIV-11	1.14	2.07	0.39	1.13	2.66	0.32				0.30	0.45	0.60	0.119 (11)	1.00
Ronda														
E3-126	1.14	2.09	0.43	1.14	2.77	0.32				0.19	0.26	0.27	0.061 (9)	1.10
E3-208	1.15	2.07	0.38	1.15	2.72	0.25				0.34	0.80	0.73	0.174 (10)	1.57
E3-227	1.15	1.97	0.35	1.15	2.27	0.39				0.31	0.88	0.55	0.171 (13)	1.13
E3-144	1.14	2.08	0.39	1.13	2.64	0.36				0.41	0.52	0.66	0.192 (10)	1.13
E3-148	1.14	2.09	0.40	1.14	2.65	0.38				0.45	0.40	0.57	0.126 (10)	1.24
Pyrenees														
Py-1	1.14	2.09	0.45	1.13	2.92	0.32				0.43	0.64	0.75	0.234 (9)	1.03
Py-18	1.16	2.14	0.41	1.14	3.01	0.21				0.31	0.70	0.69	0.239 (19)	0.94
Py-25	1.15	2.08	0.44	1.14	2.86	0.22				0.39	0.71	0.84	0.318 (18)	1.24
Py-30	1.15	2.12	0.41	1.13	2.88	0.29				0.37	0.36	0.77	0.187 (18)	1.21
Py-34	1.15	2.10	0.44	1.16	2.80	0.27				0.37	0.58	0.72	0.247 (16)	1.10
Orthopyroxene														
bbI-32e	1.10	1.88	0.24	1.11	2.16	0.29				0.27	0.89	0.30	0.028 (10)	1.22
bbI-36	1.14	1.97	0.25	1.15	2.24	0.33				0.42	0.70	0.30	0.022 (10)	2.23
bbI-37	1.14	1.95	0.22	1.14	2.18	0.27				0.17	0.70	0.35	0.057 (10)	1.25
bbI-43	1.14	1.97	0.24	1.14	2.21	0.30				0.21	0.84	0.48	0.052 (10)	2.11
bbII-13	1.13	1.94	0.23	1.15	2.22	0.30				0.27	0.93	0.30	0.017 (10)	1.91
bbII-14	1.10	1.82	0.17	1.11	2.09	0.29				0.22	0.70	0.38	0.038 (10)	1.06
bbIV-11	1.16	1.96	0.24	1.15	2.18	0.30				0.27	0.90	0.46	0.053 (10)	1.31
Ronda														
E3-126	1.14	1.93	0.22	1.15	2.20	0.24	1.16	2.53	0.33	0.27	0.70	0.40	0.052 (10)	1.52
E3-208	1.14	1.90	0.22	1.15	2.18	0.25	1.14	2.41	0.40	0.24	0.70	0.56	0.089 (10)	1.47
E3-227	1.14	1.93	0.23	1.17	2.21	0.31				0.29	1.02	0.40	0.038 (10)	1.09
E3-144	1.14	1.96	0.24	1.15	2.25	0.29				0.26	0.73	0.60	0.083 (10)	1.28
E3-148	1.14	1.94	0.24	1.15	2.23	0.32				0.26	0.82	0.55	0.061 (10)	1.24
Pyrenees														
Py-1	1.13	1.90	0.26	1.15	2.16	0.31	1.14	2.97	0.29	0.26	1.01	0.51	0.045 (10)	1.41
Py-18	1.14	1.94	0.22	1.15	2.21	0.27				0.10	0.70	0.51	0.067 (10)	1.35
Py-25	1.13	1.89	0.20	1.14	2.16	0.26	1.14	2.95	0.23	0.32	0.85	0.33	0.054 (10)	1.32
Py-30	1.15	1.94	0.20	1.15	2.19	0.27				0.09	0.70	0.44	0.058 (10)	1.49
Py-34	1.13	1.93	0.24	1.15	2.19	0.28				0.19	0.70	0.55	0.064 (10)	1.39

[a] Hyperfine parameters for spinels are from an extended Voigt-based fitting model.

in the $Fe^{3+}/\sum Fe$ determinations from the Mössbauer spectra, particularly for orthopyroxene.

A positive correlation exists between measured Fe^{3+} contents in coexisting spinel and clinopyroxene. Spinel always contains more Fe^{3+} than the coexisting clinopyroxene, particularly when calculated based on an equal number of oxygens per formula unit for both phases (e.g. a 12 oxygen basis; Fig. 4B). Most samples, including the metasomatised sample Py-25 from Caussou, yield a $D^{sp/cpx}_{Fe3+}$ in the range of 2 to 6. The couple of samples that deviate from this range in $D^{sp/cpx}_{Fe3+}$ have Cr-rich spinels, suggesting that spinel major element composition exerts an important influence on Fe^{3+} partitioning between spinel and clinopyroxene. In fact, our data set reveals a strong dependence of $D^{sp/cpx}_{Fe3+}$ on $Cr/(Cr+Al+Fe^{3+})$ in spinel (Fig. 4C). This implies that the partitioning of Fe^{3+} between spinel and clinopyroxene in the upper mantle is complex and is strongly affected by petrologic processes that cause changes in the $Cr/(Cr+Al+Fe^{3+})$ of spinel, including partial melting. Thus the partitioning behaviour of Fe^{3+} between spinel and clinopyroxene can also be influenced by the presence or absence of other phases, such as plagioclase.

4.4. Bulk rock Fe_2O_3

Combining the measured Fe^{3+} contents of orthopyroxene, clinopyroxene and spinel with their respective modal abundances permits us to determine the bulk rock Fe_2O_3 contents of our suite of samples. In addition, we can assess the relative contribution each mineral makes to the total Fe_2O_3 budget. Although orthopyroxene has the lowest $Fe^{3+}/\sum Fe$ of the three phases, it is generally a significant carrier of Fe^{3+} in these peridotite samples; in 10 of 17 samples studied, orthopyroxene contributed at least 40% of the bulk Fe_2O_3 (Fig. 5). This is due to orthopyroxene being moderately Fe-rich and having a relatively high modal abundance. Clinopyroxene usually comprises the second most abundant source of Fe^{3+}, although the contributions from spinel and clinopyroxene are often similar. Spinel, by virtue of its generally low modal abundance, contributes only about a 25% of the bulk Fe_2O_3 at most (Fig. 5). The one exception is the plagioclase-bearing sample, E3-208, where about half of the whole-rock Fe_2O_3 budget resides in spinel, although it comprises only 1 modal % of the peridotite. Several factors are responsible for this. In addition to spinel being exceedingly Fe^{3+}-rich, the modal abundances of both orthopyroxene and clinopyroxene are low (Table 1). The partitioning of Fe^{3+} between clinopyroxene and such a Cr-rich spinel also favours the latter phase (see Fig. 4C). The global Fe_2O_3 budget for sample Py-25 was calculated without considering any contribution from amphibole, since it proved impossible to obtain a clean separate for Mössbauer spectroscopy. However, since amphibole is only present in trace quantities in this sample, the overall contribution to bulk Fe_2O_3 would be minor, even if the phase were excessively Fe^{3+}-rich.

Calculated bulk Fe_2O_3 contents range from 0.03 to 0.27 wt.% (Table 3). Whole rock Fe_2O_3 is observed to decrease with increasing whole rock MgO content (Fig. 6). This is also the case for the small number of literature data available for spinel peridotite xenoliths (Canil et al., 1990; Luth and Canil, 1993; Canil et al., 1994; Canil and O'Neill, 1996). This behaviour is not unexpected due to the moderately incompatible nature of Fe^{3+} during partial melting in the spinel peridotite facies. The point labelled PUM in Fig. 6 is the primitive upper mantle value derived by Canil et al. (1994). Measured relative to this point it is clear that the orogenic peridotites, like the xenolith samples, represent variably depleted peridotite residues, including the plagioclase peridotite. In terms of the geochemical behaviour of Fe^{3+}, it can be concluded that orogenic peridotites exhibit essentially the same behaviour as spinel peridotite xenoliths.

4.5. Oxygen barometry

Oxygen fugacity, fO_2, can be estimated by considering the equilibrium between olivine, orthopyroxene and spinel:

$$6Fe_2SiO_4 + O_2 = 3Fe_2Si_2O_6 + 2Fe_3O_4 \quad (1)$$

where Fe_2SiO_4 is the fayalite component in olivine, $Fe_2Si_2O_6$ is the ferrosilite component in orthopyroxene and Fe_3O_4 is the magnetite component in spinel. The method of calculating the fO_2 follows that reported in Woodland et al. (1992), which uses the Nell–Wood calibration for reaction (1) (Wood et al., 1990). To minimise the effects of uncertainties in the temperature and pressure of equilibration, the fO_2 estimates are referenced to the fayalite–magnetite–quartz (FMQ) buffer and are reported in terms of $\Delta \log fO_2$. The consequence is that an uncertainty in temperature of 100 °C and in pressure of 3 kb translates to a difference in fO_2 of only 0.15 and 0.09 log units, respectively. Collectively these uncertainties, along with analytical uncertainties (including Fe^{3+}) yield an overall uncertainty of about ±0.5 log units in $\Delta \log fO_2$ (Woodland et al., 1992).

For our suite of samples, fO_2 can also be estimated from the Fe^{3+}-content of clinopyroxene. Luth and Canil

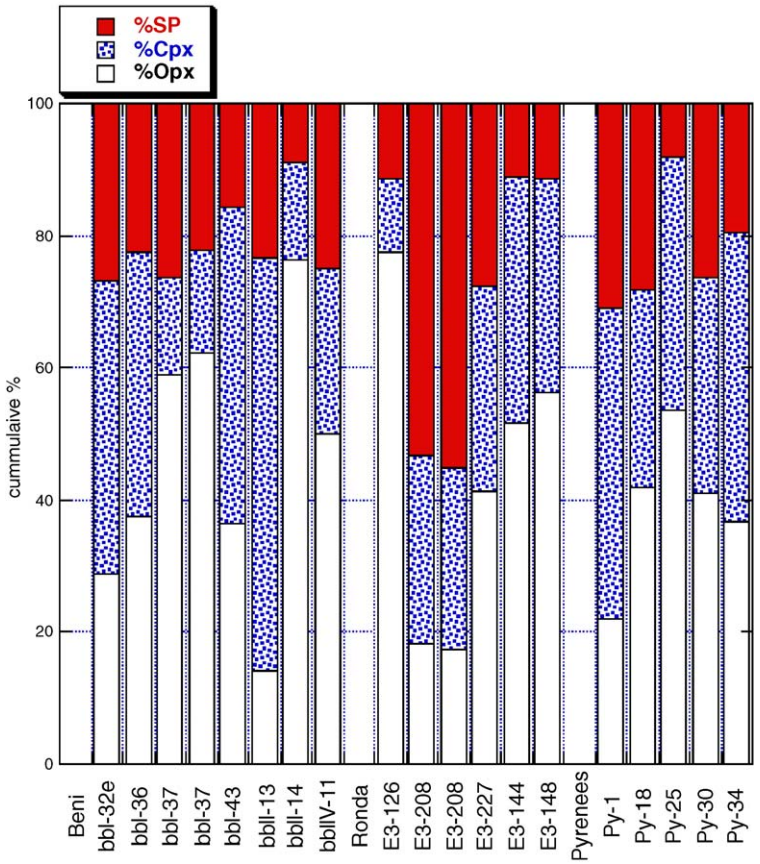

Fig. 5. Histogram depicting the relative contributions of orthopyroxene, clinopyroxene and spinel to the total bulk Fe_2O_3 content of samples in this study.

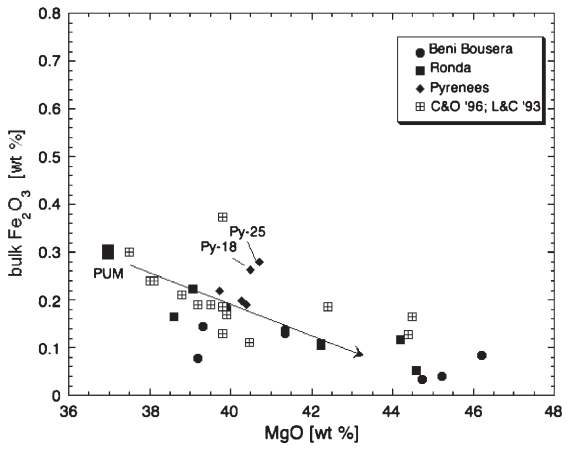

Fig. 6. Covariation of calculated bulk Fe_2O_3 with bulk rock MgO content in spinel peridotites. Literature data from Canil et al. (1994), Canil and O'Neill (1996) and by combination of data from Canil et al. (1990) and Luth and Canil (1993). PUM stands for primitive upper mantle and is taken from Canil et al. (1994). The depletion trend (arrow) represents the effect of progressive partial melt extraction.

(1993) calibrated several equilibria between clinopyroxene, orthopyroxene and olivine as oxygen barometers based upon the aegerine ($NaFe^{3+}Si_2O_6$) or essenite components ($CaFe^{3+}AlSiO_6$) in clinopyroxene. From their analysis, the equilibrium:

$$4\underset{\text{cpx}}{NaFe^{3+}Si_2O_6} + 2\underset{\text{cpx}}{CaAl_2SiO_6} + 3\underset{\text{opx}}{Fe_2Si_2O_6} = 4NaAlSi_2O_6 + 4Fe_2SiO_4 + 2CaFeSi_2O_6 + O_2 \quad (2)$$

with the assumption of ideal mixing-on-sites in the clinopyroxene yielded the most consistent results in comparison with fO_2 values obtained from the spinel-based equilibrium (1). We shall use this formulation as being representative of fO_2 values determined from the Fe^{3+} contents in clinopyroxene. Application of a regular solution model to clinopyroxene had generally a negligible effect on calculated fO_2, and in a couple of cases led to poorer agreement with the fO_2 value determined from the spinel-bearing equilibrium (1)

(Luth and Canil, 1993). As with equilibrium (1), referencing the fO_2 to the FMQ buffer mitigates the effect of uncertainties in pressure and temperature and Luth and Canil (1993) estimate of total uncertainty in of ±0.8 log units in $\Delta \log fO_2$.

The resulting fO_2 values determined from equilibria (1) and (2) are listed in Table 4. Consistent with Woodland et al. (1992), the Pyrenean massifs record generally higher fO_2 values than Ronda and Beni Bousera. The plagioclase-bearing sample, E3-208, also has a relatively high fO_2, as do other plagioclase-bearing samples from Ronda (Woodland et al., 1992). Ballhaus (1995) pointed out that higher fO_2 is to be expected in the plagioclase facies due to the concentration of Fe^{3+} into residual Cr-rich spinel, and as such, no "oxidising event" is necessary to explain the difference in relative oxygen fugacity between spinel peridotites and those from the plagioclase facies. The partitioning behaviour of Fe^{3+} illustrated in Fig. 4c will serve to exaggerate this effect as Fe^{3+} is also transferred from clinopyroxene to Cr-rich spinel. These observations imply very different relationships between partial melting and fO_2 in spinel and plagioclase peridotites. In the spinel facies, partial melting extracts Fe^{3+} from Al-rich spinel and clinopyroxene, in addition to preferentially removing these two phases from the assemblage. This leads to a decrease in bulk Fe_2O_3 and drives down fO_2 (e.g. Bryndzia and Wood, 1990, and see below). A mitigating factor would be the changing Fe^{3+}-partitioning between clinopyroxene and spinel as the spinel becomes progressively richer in Cr. On the other hand, melting in the plagioclase field could produce progressively higher fO_2 values due to the residual nature of the Cr-rich spinel and the crystal chemical affinity of Fe^{3+} for such compositions. Therefore, even in plagioclase peridotites with low bulk Fe_2O_3 contents, the fO_2 can be forced to remain high by virtue of the concentration of Fe^{3+} into the minor Cr-spinel phase. In the particular case of sample E3-208 from Ronda, which is supposed to result from melting and contamination of pre-existing lithosphere (Lenoir et al., 2001), these processes could also account for a relatively high fO_2 in this unit.

Comparison the fO_2 values determined from equilibria (1) and (2) allow us to determine whether or not spinel and clinopyroxene coexist in redox equilibrium with each other in orogenic peridotites. $\Delta \log fO_2$ values are plotted against each other in Fig. 7. Most samples from this study lie within an uncertainty envelope of ±0.8 log units, which corresponds to the uncertainty in the clinopyroxene-based equilibrium (2) given by Luth and Canil (1993).

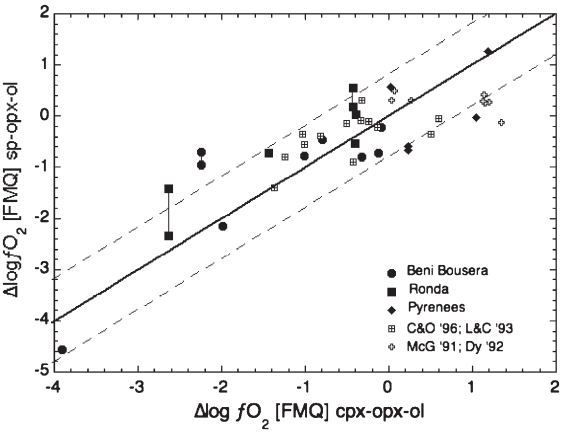

Fig. 7. Comparison of $\Delta \log fO_2$ [FMQ] values calculated using the spinel-based (Eq. (1)) and the clinopyroxene-based (Eq. (2)) oxybarometers (see text). The heavy line represents a perfect 1:1 correlation. The two dashed lines delineate an envelope of ±0.8 log units, the uncertainty in Eq. (2) reported by Luth and Canil (1993). Literature values are from McGuire et al. (1991), Dyar et al. (1992), Luth and Canil (1993) and Canil and O'Neill (1996).

In fact the combined uncertainties from both oxybarometers should be closer to ±1 log unit. It is notable that the agreement extends over a much larger range in $\Delta \log fO_2$ than the original set of samples used by Luth and Canil (1993) to test the calibration of their clinopyroxene-based oxybarometer (Fig. 7). Some scatter is apparent, but the distribution of samples indicates that there is no systematic tendency for one oxybarometer to yield fO_2 values higher than the other. Evaluation of the data in Table 4 also indicates that the magnitude of the discrepancies between the two oxybarometers bear no relation to equilibration temperature. The overall agreement between the oxybarometers leads us to conclude that orogenic peridotites do preserve redox equilibrium between spinel and clinopyroxene, although their equilibrium temperatures can be quite low. The data scatter is only slightly more than that observed for xenolith samples, which have generally equilibrated at higher temperatures. Thus, orogenic peridotites can be reliable recorders of the redox conditions reigning in the lithospheric mantle.

4.6. Controls of oxygen fugacity in spinel peridotites

There has been extensive discussion of whether the upper mantle is buffered in terms of oxygen fugacity, much focusing the relative roles of Fe and volatile elements such as C, H and S, most of which can adopt multiple valence states (e.g. Arculus, 1985; Wood et al.,

Table 4
Equilibration temperatures, computed fO_2 and calculated bulk Fe_2O_3 contents

Sample	Temperature (°C)	$\Delta \log fO_2$ sp-opx-ol (1)	$\Delta \log fO_2$ cpx-opx-ol (2)	Bulk Fe_2O_3 (wt. %)
Beni Bousera				
bbI-32e	947	−0.82	−0.32	0.145
bbI-36	920	−0.46	−0.79	0.040
bbI-37a	950	−0.70	−2.24	0.137
bbI-37b	950	−0.96	−2.24	0.130
bbI-43	1110	−0.73	−0.13	0.184
bbII-13	1137	−2.16	−1.99	0.077
bbII-14	1084	−4.56	−3.91	0.034
bbIV-11	930	−0.79	−1.0\1	0.084
Ronda				
E3-126a	915	−2.35	−2.64	0.051
E3-126b	915	−1.43	−2.64	0.054
E3-144	948	0.03	−0.40	0.224
E3-148	987	−0.73	−1.44	0.165
E3-208a	929	0.17	−0.42	0.088
E3-208b	929	0.55	−0.42	0.098
E3-227	935	−0.13	−0.40	0.117
Pyrenees				
Py-1	958	−0.22	−0.09	0.190
Py-18	986	0.57	0.02	0.263
Py-25	849	1.27	1.19	0.279
Py-30a	833	−0.60	0.23	0.197
Py-30b	833	−0.67	0.23	0.198
Py-34	903	−0.03	1.05	0.220

Temperatures computed using the BKN thermometer (Brey and Köhler, 1990). fO_2-values are computed using both equilibria (1) and (2).

1990; Ballhaus, 1993; Canil et al., 1994; McCammon and Kopylova, 2004). Comparing reconstructed bulk Fe_2O_3 contents from a suite of peridotites with plausible concentrations of C, H and S, Canil et al. (1994) concluded that mantle fO_2 was unlikely to be buffered by any single chemical system. More recently, observed variations in fO_2 beneath the Slave craton led McCammon and Kopylova (2004) to conclude that mantle fO_2 is buffered by Fe^{2+}–Fe^{3+} exchange involving spinel and/or garnet.

Our data set is well suited to further investigate the systematics of oxygen fugacity in the spinel peridotite facies of the upper mantle. From the outset it must be reiterated that equilibria that buffer oxygen fugacity, such as Eqs. (1) and (2), are really only true buffers when the pure phases are present. Then the equilibria are univariant. In the mantle, the phases are generally complex solid solutions that can adjust their compositions through numerous "sliding reactions". In this case the equilibria become multi-variant and true oxygen buffering cannot occur. Exceptions to this are graphite and diamond, which are essentially pure carbon. However, the other forms of C are indeed complex solutions, existing as a carbonate phase, a C–O–H fluid or as a dissolved component in a melt. Even at graphite saturation a coexisting C–O–H fluid can adjust its composition according a changes in fO_2 (e.g. Wood et al., 1990). This is not to say that the presence of Fe-bearing or C-bearing phases has no effect on the oxygen fugacity, particularly if the upper mantle is considered to be a closed system. The Fe^{3+} contents of spinel, clinopyroxene and orthopyroxene will change in response to perturbations in fO_2; the magnitude of this change being a function of the $Fe^{3+}/\sum Fe$-fO_2 systematics of each phase. This aspect will be explored in more detail below.

Our samples reveal a reasonable correlation between calculated $\Delta \log fO_2$ and bulk Fe_2O_3 content, suggesting

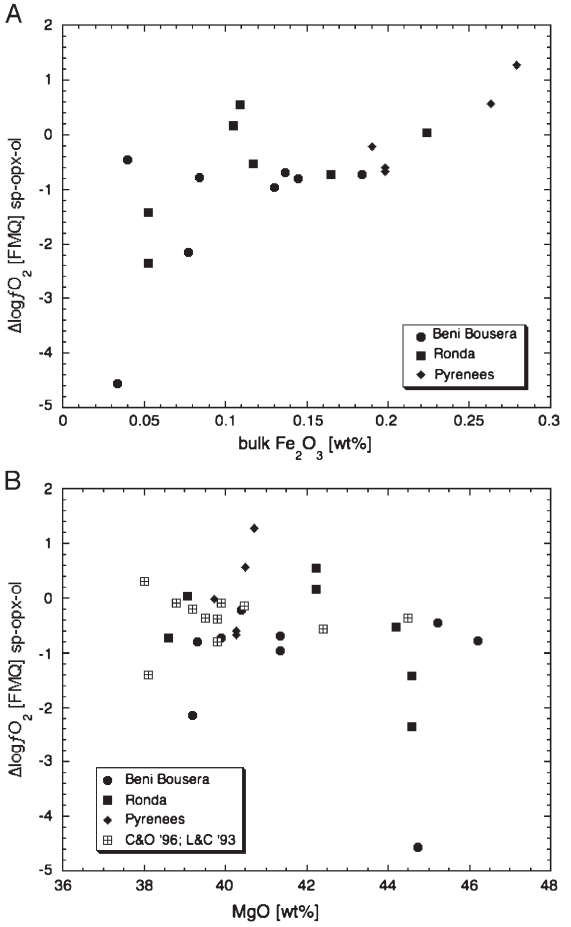

Fig. 8. Covariation of (A) calculated bulk Fe_2O_3 with $\Delta \log fO_2$ [FMQ] values calculated using the spinel-based (Eq. (1)); (B) $\Delta \log fO_2$ [FMQ] with bulk rock MgO content.

that Fe^{2+}–Fe^{3+} exchange reactions are indeed the dominant control of fO_2 in the lithospheric mantle (Fig. 8A). The covariance of spinel-based and clinopyroxene-based oxygen barometers (Fig. 7) results in similar correlations with both oxygen barometers. A relationship between $\Delta \log fO_2$ and bulk Fe_2O_3 is consistent with the notion that partial melting and melt extraction is a major process that removes Fe^{3+} from the upper mantle (Fig. 6) and contributes to a lowering of fO_2 (e.g. Bryndzia and Wood, 1990). However, the expected correlation between $\Delta \log fO_2$ and a measure of depletion, such as whole rock MgO is not observed (Fig. 8B). This lack of correlation is in fact a more graphic reflection of the data scatter exhibited in the plot of bulk MgO versus bulk Fe_2O_3 (Fig. 6). Thus our data set records a certain degree of decoupling of fO_2 from whole rock Fe_2O_3 content, which varies from locality to locality. The decoupling can be understood in terms of the bulk rock Fe_2O_3 retaining a record of partial melting, while fO_2 can be more easily influenced by subsequent geochemical processes such as metasomatism or a facies change. For example, when a previously depleted peridotite interacts with a relatively oxidised melt or fluid, the low modal abundances of spinel and clinopyroxene can be easily reset, resulting in only a minor change in bulk Fe_2O_3 content although the increase in fO_2 could be significant. This behaviour is analogous to the V-fO_2 systematics documented by Lee et al. (2003). However, bulk rock Fe_2O_3 is a less robust parameter than V for monitoring partial melting since modal metasomatism can often involve the addition of Fe^{3+}, which can re-establish the coupling between bulk Fe_2O_3 and fO_2 (e.g. sample Py-25). As previously discussed, the peridotites from the plagioclase facies record rather high fO_2-values merely due to the concentration of Fe^{3+} in residual Cr-rich spinel, yet the bulk Fe_2O_3 content of sample E3-208 is not anomalously high (Table 4).

4.7. Modelling the relationship between Fe^{3+} in spinel and fO_2

A further question related to the control of fO_2 in the mantle is how spinel peridotite might respond to oxidation, for example during a metasomatic event. What influence could Fe^{3+}–Fe^{2+} equilibria have on the fO_2 in such a case? We can address this by exploring the $Fe^{3+}/\sum Fe$-fO_2 systematics of spinel that are reflected through the variation in magnetite activity with changing Fe^{3+} content and the subsequent effect this has on fO_2 via Eq. (1). To do this, we have modelled the oxidation of spinel from two samples; BB-II-14, which records the lowest fO_2 in our data set and BB-I-37a, which has a high Cr-content. The oxidation is simulated by progressively converting Fe^{2+} to Fe^{3+} in steps of 0.005 cations per formula unit. To maintain charge and mass balance, Cr and Al are removed in amounts necessary to preserve the initial Cr/Al, and Mg is added to compensate for the converted Fe^{2+}. Here it is assumed that the large reservoir of neighbouring olivine can provide this small amount of Mg without changing its composition. The new activity of magnetite in spinel is computed at each step and this is used to calculate the resulting fO_2. The results reveal that the effects of an incremental increase in Fe^{3+} in spinel are far from linear (Fig. 9). At low overall Fe^{3+} contents, large changes in fO_2 can be achieved. However, at about FMQ, the activity–composition relations in spinel are such that progressively more and more Fe^{3+} must be added to cause even a small change in fO_2. A quasi-limit is reached at $\Delta \log fO_2 \sim FMQ+1$. This result explains why reports of spinel peridotites with high fO_2-values (e.g. at Ni–NiO) are so rare. In addition, we can better understand why continental lithosphere records fO_2-values near FMQ, even in many depleted harzburgitic compositions; the re-setting of fO_2 via cryptic or modal metasomatism is relatively effective in a reduced peridotite. This calculation indicates that although fO_2 is not strictly buffered by a multi-variant equilibrium between olivine–orthopyroxene and spinel, Fe^{3+}–Fe^{2+} equilibria can indeed have an important influence on fO_2.

These considerations indicate that the control of fO_2 in the spinel peridotite facies is complex and is sensitive to local variations in bulk composition (degree of

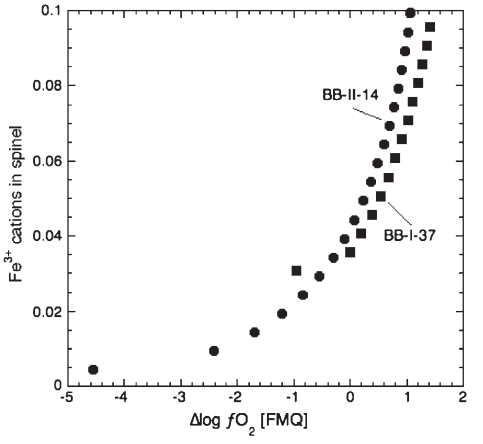

Fig. 9. Change in $\Delta \log fO_2$ resulting from a simulated stepwise oxidation of spinel. Two spinels with different Cr contents are modelled (BB-II-14 and BB-I-37a). See text for details of calculation. Note the quasi-limit in fO_2 with increasing Fe^{3+} content in spinel.

depletion). For example, a metasomatic event will have a different effect on resetting the fO_2 recorded in a harzburgite compared to a fertile lherzolite. This observation, combined with the fact that metasomatism is spatially heterogeneous, provides an explanation for the absence of any systematic fO_2-gradients in the Beni Bousera, Ronda, or Lherz massifs (Woodland et al., 1992). From the current study, the implication is that Fe^{3+}–Fe^{2+} equilibria have an important, if not dominant influence on fO_2. Even where C, H and/or S have a role to play, it will be equilibria between these volatile elements and Fe^{3+}–Fe^{2+} in spinel and the pyroxenes that will locally define the fO_2.

Acknowledgements

This research was supported in part by the Bayerisches Geoinstitut. F. Seifert and C. McCammon are thanked for access to the Mössbauer laboratory at the Geoinstitut and for stimulating discussions, particularly concerning the fitting of Mössbauer spectra. R. Altherr is also thanked for his support of this work, both in substance and in inspiration. The Mössbauer laboratory in Frankfurt was established through the financial assistance of the Deutsche Forschungsgemeinschaft (DFG). The manuscript greatly benefited from the thoughtful comments of D. Canil and an anonymous reviewer.

Appendix A. Treatment of Mössbauer spectra

Spinel spectra are essentially composed of two broad absorption peaks and were initially fit using two quadrupole split Lorentzian doublets for Fe^{2+} and one doublet for Fe^{3+}; the high and low velocity components having equal areas and line widths (Wood and Virgo, 1989). Although this approach yielded a reasonable fit to the spectra, a small misfit was usually apparent in the shoulder regions of the absorption peaks, suggesting a Gaussian component to the peak shape (Fig. A1A). A spectral model using extended Voigt-based fitting (xVBF, Lagarec and Rancourt, 1997) for the two Fe^{2+} components and a regular Lorentzian doublet for Fe^{3+} was found to produce a significantly improved fit for all spinel samples ($\chi^2 < 1.2$ compared with values of up to 2.7 for the fits with pure Lorentzian line shapes), and was adopted in this study (Fig. A1B). To limit the number of fit

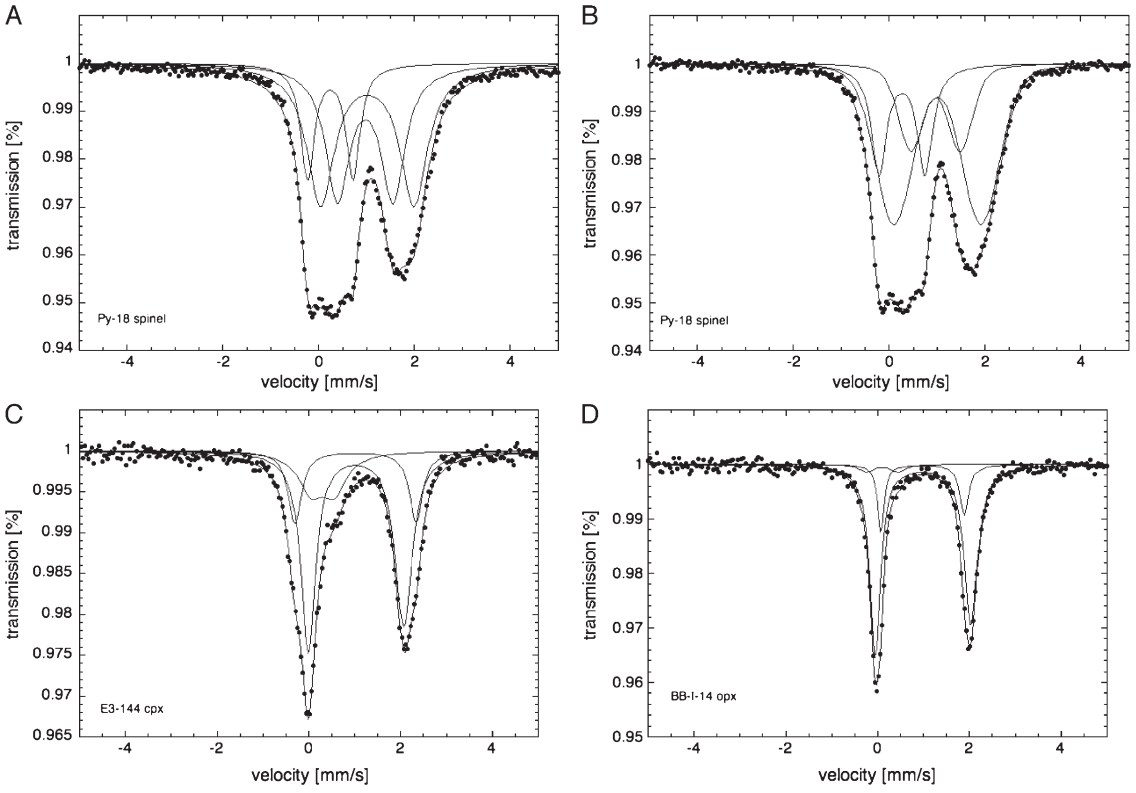

Fig. A1. Mössbauer spectra of (A) spinel Py-18 fit using Lorentzian peak shapes, (B) spinel Py-18 fit using the extended Voigt-based fitting model. Note the improvement in the fit to the data: (C) clinopyroxene E3-144 and (D) orthopyroxene BB-II-14.

parameters, the line widths of the two Fe^{2+} components were constrained to be equal. Hyperfine parameters are listed in Table 3.

Spectra from clinopyroxene were fit following the approach successfully applied by Woodland and Peltonen (1999) for mantle clinopyroxenes, which is similar to the spectral model adopted by others (e.g. Luth and Canil, 1993; Canil and O'Neill, 1996; McCammon et al., 1998; Sobolev et al., 1999). The spectra were fit with two quadrupole split doublets for Fe^{2+} and one doublet for Fe^{3+}, each with Lorentzian peak shapes and equal areas. Peak widths were allowed to vary for the Fe^{2+} doublets, to help account for next-nearest-neighbour effects. However, in most spectra, the Fe^{2+} doublet with the larger quadrupole splitting was clearly subordinate in area and was constrained to have equal peak widths. Allowing variable widths for the high and low velocity components of this doublet produced either no appreciable change to the fit or led to instabilities in the fitting procedure and subsequently unacceptably large uncertainties in the derived hyperfine parameters. So in practice, only the line width of the dominant Fe^{2+} doublet was permitted to vary. The refined $Fe^{3+}/\sum Fe$ values obtained here were somewhat lower than those derived from a more typical spectral model with the constraint of equal line widths. Although the two Fe^{2+} doublets can be generally attributed to Fe^{2+} occupying the M1 and M2 sites in the pyroxene structure, the goal of this study was to obtain a robust measure of $Fe^{3+}/\sum Fe$ rather than to assess the crystal chemistry of Fe in these complex solid solutions. Furthermore, difficulties in using the relative areas of Fe^{2+} doublets as a measure of Fe^{2+} partitioning between the M1 and M2 sites has been repeatedly documented (Dowty and Lindsley, 1973; Virgo, 1973; McCallister et al., 1976). Therefore, the relative areas of the Fe^{2+} doublets need not reflect the actual intersite distribution of Fe^{2+}. Likewise, the spectra were not of sufficient resolution to allow the fitting of separate doublets for both tetrahedrally and octahedrally coordinated Fe^{3+}. In several cases, one of the hyperfine parameters for the Fe^{3+} doublet had to be constrained to obtain reasonable values for the other parameters. Although there was no obvious misfit to the spectra, the clinopyroxene spectra were also fit using the xVBF method in an analogous manner as for spinel. This approach yielded a statistically better fit for 7 out of 17 spectra analysed in this study. For the remaining samples, the xVBF method produced statistically equivalent or worse fits than those obtained assuming Lorentzian line shapes, as previously described. The relative areas of the two Fe^{2+} doublets computed by the xVBF model varied tremendously between samples and were generally subject to large errors, indicating significant correlation between the hyperfine parameters. For some samples, the derived hyperfine parameters were subject to excessively large errors, further suggesting problems with fit-parameter correlation. Considering these observations, we opted for the spectral model with Lorentzian line shapes and variable line width for one of the Fe^{2+} doublets. This model has been successfully applied by a number of workers, including the first author, to a large number of mantle-derived clinopyroxenes, as mentioned above. A representative spectrum from a clinopyroxene is presented in Fig. A1C and hyperfine parameters are listed in Table 3.

Orthopyroxene spectra were fit in a similar fashion as clinopyroxene with two quadrupole split doublets for Fe^{2+} and one doublet for Fe^{3+}, each with Lorentzian peak shapes and equal areas. Good results were obtained by relaxing the constraint of equal line widths for the high and low velocity components of the Fe^{2+} doublets, to help account for next-nearest-neighbour effects (e.g. Fig. A1D). In a couple of instances the addition of a third Fe^{2+} doublet with a large quadrupole splitting was necessary to obtain a reasonable fit (see Seifert, 1983; Luth and Canil, 1993). The poor resolution of the Fe^{3+} doublet often necessitated the fixing of one or more of the hyperfine parameters for this component. Most frequently the quadrupole splitting was fixed at a value of 0.7 mm/s (Seifert, 1983). Derived hyperfine parameters are given in Table 3. An alternative model of Voigt-based fitting proved to be less satisfactory for the orthopyroxene spectra.

References

Arculus, R.J., 1985. Oxidation status of the mantle: past and present. Annu. Rev. Earth Planet. Sci. 13, 75–95.

Ballhaus, C., 1993. Redox states of lithospheric and asthenospheric mantle. Contrib. Mineral. Petrol. 114, 331–348.

Ballhaus, C., 1995. Is the upper mantle metal saturated? Earth Planet. Sci. Lett. 132, 75–86.

Bodinier, J.L., Guiraud, M., Fabriès, J., Dostal, J., Dupuy, C., 1987. Petrogenesis of layered pyroxenites from the Lherz, Freychinède and Prades ultramafic bodies (Ariège, Franch Pyrenees). Geochim. Cosmochim. Acta 51, 279–290.

Brey, G.P., Köhler, T., 1990. Geothermobarometry in four-phase lherzolites: II. New thermobarometers, and practical assessment of existing thermobarometers. J. Petrol. 31, 1353–1378.

Bryndzia, L.T., Wood, B.J., 1990. Oxygen thermobarometry of abyssal spinel peridotites: the redox state and C–O–H volatile composition of the Earth's sub-oceanic upper mantle. Am. J. Sci. 290, 1093–1116.

Canil, D., O'Neill, H.St.C., 1996. Distribution of ferric iron in some upper-mantle assemblages. J. Petrol. 37, 609–635.

Canil, D., Virgo, D., Scarfe, C.M., 1990. Oxidation state of mantle xenoliths from British Columbia, Canada. Contrib. Mineral. Petrol. 104, 453–462.

Canil, D., O'Neill, H.St.C., Pearson, D.G., Rudnick, R., McDonough, W.F., Carswell, D.A., 1994. Ferric iron in peridotites and mantle oxidation states. Earth Planet. Sci. Lett. 123, 205–220.

Conquéré, F., 1977. Pétrologie des pyroxenites litées dans les complexes ultramafiques de l'Ariège (France) et autre gisements de lherzolite à spinelle. Compositions minèralogiques et chimiques, évolution des conditions d'équilibre des pyroxenites. Bull. Soc. Fr. Minéral. Cristallogr. 100, 42–80.

Conquéré F., 1978. Pétrologie de complexes ultrmafiques de lherzolites à spinelle de l'Ariège (France). Unpublished Thèse Doc. d'Etat, Univ. Paris VI, 333 pp.

Conquéré, F., Fabriès, J., 1984. Caractères pétrographiques et chimiques des péridotites à spinelle des gisements ultramafiques des Lherz et de Freychinède (Ariège, Pyrénées Françaises). Kimberlites III. Ann. Sci. Univ. Clermont-Ferand II 74, 55–83.

Dick, H.J.B., Fisher, R.L., 1984. Mineralogical studies of residues of mantle melting: abyssal and alpine-type peridotites. In: Kornprobst, J. (Ed.), Kimberlites II. Dev. Petrol. Ser. V, vol. 11B. Elsevier, Amsterdam, pp. 295–308.

Dowty, E., Lindsley, D.H., 1973. Mössbauer spectra of synthetic hedenbergite–ferrosilite pyroxenes. Am. Mineral. 58, 850–868.

Dyar, M.D., McGuire, A.V., Ziegler, R.D., 1989. Redox equilibria and chemistry of coexisting minerals from spinel lherzolite xenoliths. Am. Mineral. 74, 969–980.

Dyar, M.D., McGuire, A.V., Harrell, M.D., 1992. Crystal chemistry of iron in two styles of metasomatism in the upper mantle. Geochim. Cosmochim. Acta 56, 2579–2586.

Fabriès, J., 1979. Spinel–olivine geothermometry in peridotites from ultramafic complexes. Contrib. Mineral. Petrol. 69, 329–336.

Fabriès, J., Bodinier, J.L., Dupuy, C., Lorand, J.P., Benkerrou, C., 1989. Evidence for modal metasomatism in the orogenic spinel lherzolite body from Caussou (Northeastern Pyrenees, France). J. Petrol. 30, 199–228.

Fabriès, J., Lorand, J.P., Bodinier, J.L., Dupuy, C., 1991. Evolution of the upper mantle beneath the Pyrenees: evidence from orogenic spinel lherzolite massifs. J. Petrol. Spec. Lherzolite Iss. 55–76.

Frey, F.A., Suen, C.J., Stockman, H.W., 1985. The Ronda high temperature peridotite: geochemistry and petrogenesis. Geochim. Cosmochim. Acta 49, 2469–2491.

Huckenholz, H.G., Schairer, J.F., Yoder Jr., H.S., 1969. Synthesis and stability of ferri-diopside. Min. Soc. Am. Spec. Paper 2, 163–177.

Kornprobst, J., 1969. Le massif ultrabasique de Beni Bousera. Etude des péridotites de haute température et de haute pression et des pyroxenites avec ou sans grenat qui leur sont associées. Contrib. Mineral. Petrol. 23, 283–322.

Kornprobst, J., Ohnenstetter, D., Ohnenstetter, M., 1981. Na and Cr contents in clinopyroxenes from peridotites: a possible discriminant between "sub-continental" and "sub-oceanic" mantle. Earth Planet. Sci. Lett. 53, 241–254.

Lagarec, K., Rancourt, D.G., 1997. Extended Voigt-based analytic lineshape method for determining *N*-dimensional correlated hyperfine parameter distributions in Mössbauer spectroscopy. Nucl. Instrum. Methods Phys. Res., B 129, 266–280.

Lee, C.-T.A., Brandon, A.D., Norman, M., 2003. Vanadium in peridotites as a proxy for paleo-fO_2 during partial melting: prospects, limitations, and implications. Geochim. Cosmochim. Acta 67, 3045–3064.

Lenoir, X., Garrido, C.J., Bodinier, J.L., Dautria, J.M., Gervilla, F., 2001. The recrystallisation front of the Ronda peridotite: evidence for melting and thermal erosion of subcontinental lithospheric mantle beneath the Alboran Basin. J. Petrol. 42, 141–158.

Li, J.-P., 1991. Evolution chimique des phases solides dans la fusion partielle ete la reéquilibration de subsolidus des péridotites naturelles: étude experimentale et applications. unpub. PhD thesis, Université de Clermont-Ferrand II, France, DU380, p. 262.

Li, J.-P., Kornprobst, J., Vielzeuf, D., 1995. An improved experimental calibration of the olivine–spinel geothermometer. Chin. J. Geochem. 14, 68–77.

Luth, R.W., Canil, D., 1993. Ferric iron in mantle-derived pyroxenes and a new oxybarometer for the mantle. Contrib. Mineral. Petrol. 113, 236–248.

McCallister, R.H., Finger, L.W., Ohashi, Y., 1976. Intracrystalline Fe^{2+}–Mg equilibria in three natural Ca-rich clinopyroxenes. Am. Mineral. 61, 671–676.

McCammon, C.A., Kopylova, M.G., 2004. A redox profile of the Slave mantle and oxygen fugacity control in the cratonic mantle. Contrib. Mineral. Petrol. 148, 55–68.

McCammon, C.A., Chinn, I.L., Gurney, J.J., McCallum, M.E., 1998. Ferric iron content of mineral inclusions in diamond from George Creek, Colorado determined using Mössbauer spectroscopy. Contrib. Mineral. Petrol. 133, 30–37.

McGuire, A.V., Dyar, M.D., Nielson, J.E., 1991. Metasomatic oxidation of upper mantle peridotite. Contrib. Mineral. Petrol. 109, 252–264.

Nakamura, A., Schmalzried, H., 1983. On the stoichiometry and point defects of olivine. Phys. Chem. Miner. 10, 27–37.

Obata, M., 1980. The Ronda peridotite: garnet–spinel– and plagioclase–lherzolite facies and P–T trajectories of a high temperature intrusion. J. Petrol. 21, 533–572.

O'Neill, H.St.C., Wall, V.J., 1987. The olivine–orthopyroxene–spinel oxygen geobarometer, the nickel precipitation curve and the oxygen fugacity of the Earth's upper mantle. J. Petrol. 28, 1169–1191.

O'Neill, H.St.C., Rubie, D.C., Canil, D., Geiger, C.A., Ross II, C.R., Seifert, F., Woodland, A., 1993. Ferric iron in the upper mantle and transition zone assemblages: implications for relative oxygen fugacities in the mantle. Evolution of the Earth and Planets. Geophys. Monogr. 74, vol 14. IUGG, pp. 73–88.

Pearson, D.G., Davies, G.R., Nixon, P.H., 1993. Geochemical constraints on the petrogenesis of diamond facies pyroxenites from the Beni Bousera peridotite massif, Northern Morocco. J. Petrol. 34, 125–172.

Seifert, F., 1983. Mössbauer line-broadening in aluminous orthopyroxenes: evidence for next-nearest-neighbour interactions and short-range order. Neues Jahrb. Mineral. Abh. 148, 141–162.

Seitz, H.-M., Woodland, A.B., 2000. The distribution of lithium in peridotitic and pyroxenitic mantle lithologies–an indicator of magmatic and metasomatic processes. Chem. Geol. 166, 47–64.

Sobolev, V.N., McCammon, C.A., Taylor, L.A., Snyder, G.A., Sobolev, N.V., 1999. Precise Mössbauer milliprobe determination of ferric iron in rock-forming minerals and limitations of electron microprobe analysis. Am. Mineral. 84, 78–85.

Van der Wal, D., Vissers, R.L.M., 1996. Structural geology of the Ronda peridotite, SW Spain: deformation history. J. Petrol. 37, 23–43.

Virgo, D., 1973. The ^{57}Fe Mössbauer spectra of synthetic pyroxenes across part of the join Fs_{85}–En_{15}–Wollastonite. Yearb.-Carnegie Inst. Wash. 72, 540–544.

Wood, B.J., Virgo, D., 1989. Upper mantle oxidation state: ferric iron contents of lherzolite spinels by ^{57}Fe Mössbauer spectroscopy and resultant oxygen fugacities. Geochim. Cosmochim. Acta 53, 1277–1291.

Wood, B.J., Bryndzia, L.T., Johnson, K.E., 1990. Mantle oxidation state and ist relation to tectonic environment. Science 248, 337–345.

Woodland, A.B., Angel, R.J., 2000. Phase relations in the system fayalite–magnetite at high pressures and temperatures. Contrib. Mineral. Petrol. 139, 734–747.

Woodland, A.B., Peltonen, P., 1999. Ferric iron contents of garnet and clinopyroxene and estimated oxygen fugacities of peridotite xenoliths from the Eastern Finland Kimberlite Province. P.H. Nixon Volume Proc. 7th Kimberlite Conference. Redroof Publishers, Cape Town, SA, pp. 904–911.

Woodland, A., Kornprobst, J., Wood, B.J., 1992. Oxygen thermobarometry of orogenic lherzolite massifs. J. Petrol. 33, 203–230.

Woodland, A.B., Kornprobst, J., McPherson, E., Bodinier, J.-L., Menzies, M.A., 1996. Metasomatic interactions in the lithospheric mantle: petrologic evidence from the Lherz Massif, French Pyrenees. Chem. Geol. 134, 83–112.